ISSN 1063-7834, Physics of the Solid State, 2018, Vol. 60, No. 3, pp. 520–526. © Pleiades Publishing, Ltd., 2018.
Original Russian Text © N.S. Pavlovskii, A.A. Dubrovskii, S.E. Nikitin, S.V. Semenov, K.Yu. Terent'ev, K.A. Shaikhutdinov, 2018, published in Fizika Tverdogo Tela, 2018, Vol. 60, No. 3, pp. 515–520.

MAGNETISM

Magnetostriction of Hexagonal $HoMnO_3$ and $YMnO_3$ Single Crystals

N. S. Pavlovskii[a, b, *], A. A. Dubrovskii[a, c], S. E. Nikitin[d, e], S. V. Semenov[a, b], K. Yu. Terent'ev[a], and K. A. Shaikhutdinov[a]

[a] *Kirensky Institute of Physics, Federal Research Center KSC, Siberian Branch, Russian Academy of Science, Krasnoyarsk, 660036 Russia*

[b] *Siberian Federal University, Krasnoyarsk, 660041 Russia*

[c] *International Laboratory of High Magnetic Fields and Low Temperatures, Wroclaw, Poland*

[d] *Max Plank Institute for Chemical Physics of Solids, Dresden, Germany*

[e] *Institute of Solid State Physics, Dresden Technical University, Dresden, Germany*

**e-mail: nspav1991@gmail.com*

Received September 4, 2017

Abstract—We report on the magnetostriction of hexagonal $HoMnO_3$ and $YMnO_3$ single crystals in a wide range of applied magnetic fields (up to $H = 14$ T) at all possible combinations of the mutual orientations of magnetic field H and magnetostriction $\Delta L/L$. The measured $\Delta L/L(H, T)$ data agree well with the magnetic phase diagram of the $HoMnO_3$ single crystal reported previously by other authors. It is shown that the nonmonotonic behavior of magnetostriction of the $HoMnO_3$ crystal is caused by the Ho^{3+} ion; the magnetic moment of the Mn^{3+} ion parallel to the hexagonal crystal axis. The anomalies established from the magnetostriction measurements of $HoMnO_3$ are consistent with the phase diagram of these compounds. For the isostructural $YMnO_3$ single crystal with a nonmagnetic rare-earth ion, the $\Delta L/L(H, T)$ dependences are described well by a conventional quadratic law in a wide temperature range (4–100 K). In addition, the magnetostriction effect is qualitatively estimated with regard to the effect of the crystal electric field on the holmium ion.

DOI: 10.1134/S1063783418030228

1. INTRODUCTION

In the last few decades, multiferroics combining the magnetic ordering with ferroelectricity have been intensively investigated due to their potential application in functional elements, converters, and data storage devices [1–5]. The attention to these materials is related to the possible control of the electrical properties of these compounds by a magnetic field and vice versa; therefore, it is interesting to examine the main possible mechanisms of their interplay at the microscopic level.

The $RMnO_3$ (R = Gd–Lu, Y, or Sc) manganites are multiferroics [6, 7]. These materials can crystallize in the two structural types: rhombic or hexagonal. The ordering type depends on the rare-earth element radius. When R is the ion with a small ionic radius (R = Ho–Lu, Y, Sc, or In), $RMnO_3$ crystallizes in the hexagonal packing with the specific gravity $P63cm$. When R is the ion with a large ionic radius (R = Gd–Dy), $RMnO_3$ crystallizes in the orthorhombic structure with the specific gravity $Pbnm$. In addition, as was found in [8], hexagonal $RMnO_3$ with a small radius of ion R becomes orthorhombic if the high pressure (4 GPa) and high temperature (1000°C) are simultaneously used [8]. The systems of both types were investigated in detail in [1, 2, 6–18].

The magnetic phase diagrams of hexagonal $RMnO_3$ are fairly complex [6, 7, 11]. It was concluded that these systems have at least two magnetic ordering types related to the 4f and 3d subsystems. In addition, it is well-known that the hexagonal manganites are antiferromagnets, as well as ferroelectrics with the high ferroelectric ordering temperatures in the range from 590 to 1000 K. The antiferromagnetic order is established at low temperatures (below 100 K) and coexists with ferroelectricity.

Hexagonal $HoMnO_3$ is a ferroelectric below 830 K and an antiferromagnet below $T_N \sim 76$ K. As follows from the data reported in [6], the manganese magnetic moments can occupy two positions: in the $P\underline{6}3\underline{c}m$ magnetic structure ($33\ \text{K} < T < T_N$) in zero external magnetic field (the Mn^{3+} ion spins are perpendicular to the hexagonal crystal axis) and in the $P\underline{6}3c\underline{m}$ configuration ($5.2\ \text{K} < T < 33\ \text{K}$) in zero external magnetic

field (the Mn spins are parallel to the hexagonal crystal axis). The magnetic structure of the intermediate phase is described by the $P\underline{6}_3$ symmetry group, which has the lower magnetic anisotropy [6, 7]. In addition, in the specific gravity $P\underline{6}3c\underline{m}$, possibly only a third of Mn^{3+} ion spins are directed along the hexagonal crystallographic axis, whereas in the $P\underline{6}3\underline{c}m$ phase the Mn^{3+} spins are rotated in the plane by 90° [19–21].

However, the role of Ho^{3+} ions in the magnetic ordering of the $HoMnO_3$ single crystal remains unclear. Most data are indicative of the fact that the Ho^{3+} moments align along the hexagonal axis. Sugie et al. [22] proposed the model of noncollinearity of ordering of Ho^{3+} ions in the hexagonal plane. In addition, the neutron scattering experiments suggested the antiferromagnetic ordering of a part of Ho^{3+} moments along the hexagonal axis in the region below or close to the temperature of spin reorientation of Mn^{3+} ions [23, 24].

Symmetry of the hexagonal $HoMnO_3$ single crystals forbids the direct magnetoelectric interaction; therefore, it is reasonable to explain this coupling by the magnetoelastic effect [25]. As was mentioned in [6], the phase diagram in itself is insufficient to establish whether the magnetoelastic coupling plays a decisive role. For this reason, it was necessary to measure the magnetostriction effect. However, in [6, 7], these measurements were only performed for one direction in the hexagonal $HoMnO_3$ single crystal. In addition, the applied fields were insufficient and corresponded to a small part of the magnetic phase diagram.

In this work, we measured the magnetostriction effect with all (five) possible configurations magnetic field–$\Delta L/L$ in applied magnetic fields of up to 14 T in a wide temperature range. In addition, to elucidate the role of Ho^{3+} ions, we performed the analogous measurements on the hexagonal $YMnO_3$ single crystals, i.e., on the single crystal with magnetic Ho^{3+} ions replaced by nonmagnetic Y^{3+} ions. This approach was used earlier in studying the bulk magnetic coupling constants in $YbInCu_4$ [26].

2. EXPERIMENTAL

High-quality $HoMnO_3$ and $YMnO_3$ hexagonal single crystals were grown by optical zone melting using a Crystal System Corp. FZ-4000 four-mirror furnace. The growth conditions were almost identical to those described in [27]. The obtained rods were first very fragile; therefore, the samples were annealed in air for 8 h at a temperature of $t = 800$°C and then cooled in the furnace. X-ray diffraction analysis confirmed that the lattice parameters of the single crystal correspond to those reported in [27]. The X-ray fluorescence data showed that after the second centimeter of the growth, the Ho : Mn and Y : Mn ratios became equal to unity and remained invariable for the rest of the growth time. The samples were oriented along the Kikuchi lines using scanning electron microscopy. Then, cubic samples were cut from the rod and oriented along the orthogonal crystallographic axes c, a, and b', where c is the six-order symmetry axis, a is the second-order axis, and b' is perpendicular to a and c. The magnetic measurements were performed on a Quantum Design PPMS 6000 facility and a vibrating sample magnetometer [28]. The magnetostriction was measured at the Laboratory of High Magnetic Fields and Low Temperatures (Wroclaw, Poland) on an experimental setup based on an Oxford 15 T superconducting solenoid [29]. The magnetostriction was measured for five configurations of the directions between the striction effect ($\Delta L/L$) and applied magnetic field (H) for the $HoMnO_3$ crystal and three configurations of the $YMnO_3$ single crystal.

3. RESULTS AND DISCUSSION

Figure 1 shows magnetization M as a function of applied magnetic field H in the $HoMnO_3$ single crystal at different temperatures. When the magnetic field is applied along the hexagonal c axis, the magnetization curve exhibits the behavior typical of the spin-flop transition. The $M(H)$ dependences become monotonic above 30 K, which is the temperature at which the magnetic crystal symmetry group changes from $P\underline{6}3c\underline{m}$ to $P\underline{6}3\underline{c}m$. When the magnetic field is applied along the a axis, the $M(H)$ plots contain no features. These results agree well with the data from [22].

Figure 2 shows the temperature dependence of the magnetic moment in an applied magnetic field of $H = 0.1$ T. Obviously, the critical points in the plot are observed when the magnetic field is applied along the c axis. The first such point near $T = 4.7$ K corresponds to the first reorientation of manganese moments and/or ordering of Ho^{3+} ions [7]. The second point at $T = 37$ K corresponds to the reorientation of manganese ions from the $P\underline{6}3\underline{c}m$ to $P\underline{6}3c\underline{m}$ configuration. The Neel temperature corresponding to the ordering of manganese ions at $T = 76$ K is not clearly seen, because of the strong paramagnetic contribution of Ho^{3+} ions. When the applied magnetic field is directed along the second-order axis, the $M(H)$ plot contains no anomalies.

The transverse magnetostriction of the $HoMnO_3$ single crystal is illustrated in Fig. 3. One can see the nonmonotonic behavior of the magnetostriction for all the three possible configurations of the magnetic field direction (striction, Fig. 3). The magnetostriction is minimum in the temperature range of $T = 4.2$–6 K, i.e., near the first critical point in the $M(H)$ dependence (Fig. 2), which, as was mentioned above, corresponds to the first reorientation of the manganese moments or ordering of Ho^{3+} ions. In this configuration, the magnetostriction is $\sim 10^{-5}$, which is typical

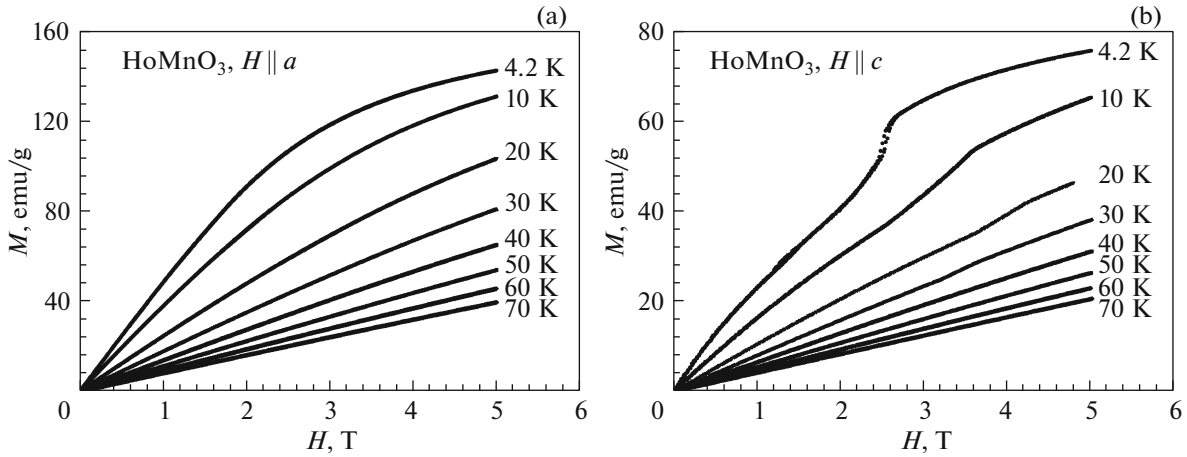

Fig. 1. Dependence of magnetic moment M on magnetic field H at different temperatures along the a and c axes for the hexagonal $HoMnO_3$ single crystal.

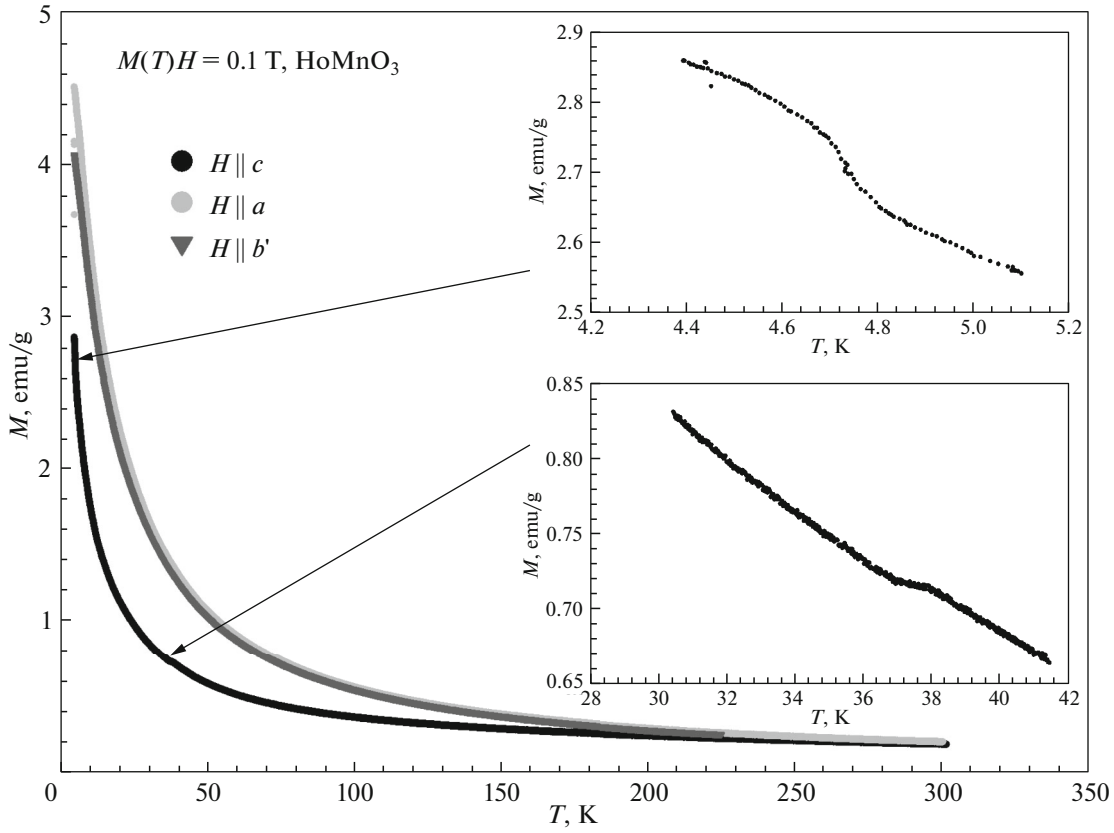

Fig. 2. Temperature dependence of magnetization M in a magnetic field of $H = 0.1$ T along three crystallographic axes. Inset: details of magnetization near the critical temperatures along the c axis.

of 4*f* and 3*d* elements. Both the manganese and holmium ion can be responsible for this effect.

Figure 4 shows the longitudinal magnetostriction effect in the $HoMnO_3$ single crystal. The low-temperature portion of the plots was described well in [6, 7] for the $\Delta L/L \parallel c$ and $H \parallel c$ configurations; however, the behavior of magnetostriction in the range of strong (over 7 T) magnetic fields was not presented in these

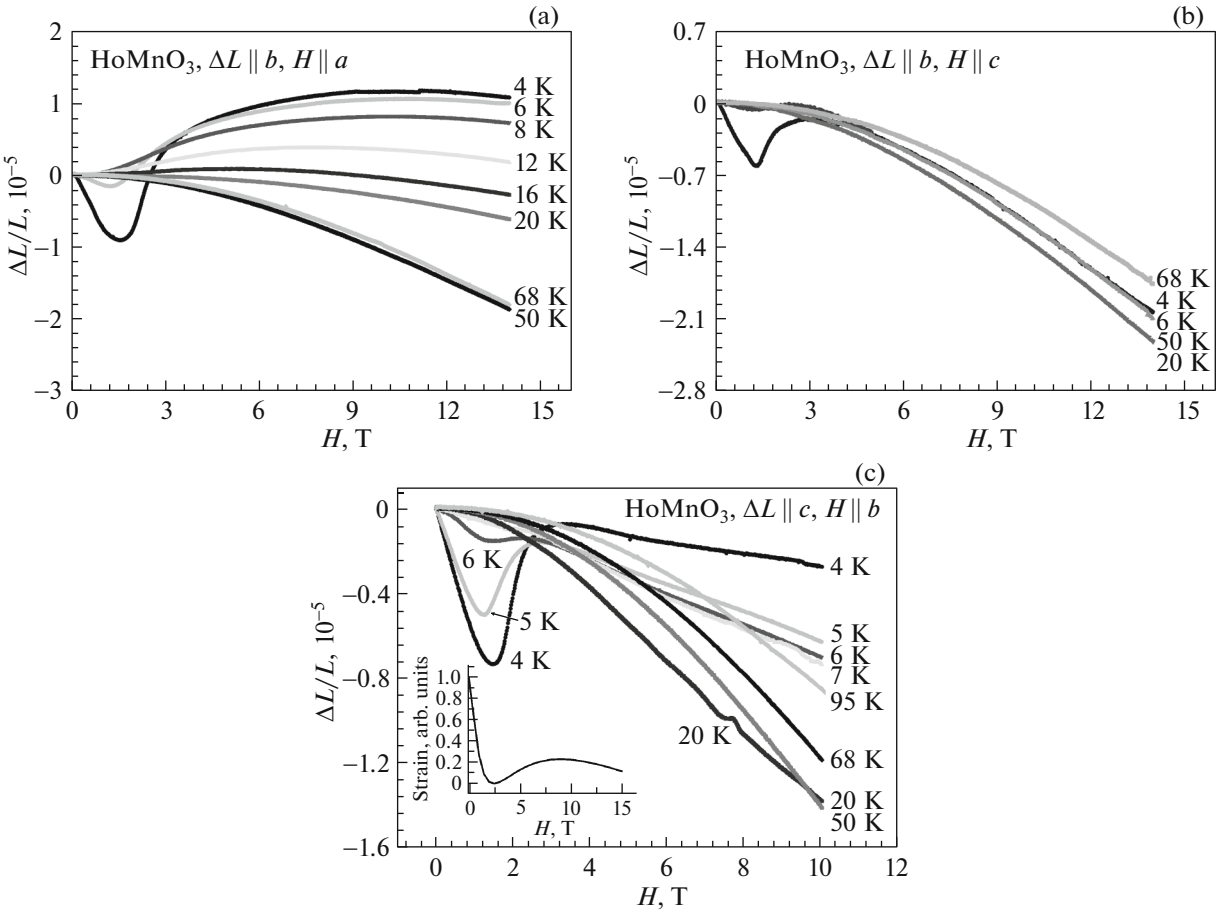

Fig. 3. Transverse magnetostriction of $HoMnO_3$ at different temperatures in different configurations. Inset: calculated magnetostriction of the Ho^{3+} subsystem in the crystal electric field approximation.

works. It can be seen from our data that after the growth of magnetostriction and attaining the smooth maximum, the magnetostriction decreases both along the six- and second-order axes. In addition, note that in the *cc* configuration in a field of $H = 14$ T, the magnetostriction changes its sign. At temperatures above $T = 30$ K, the plot has no anomalies. Another important moment is that the effect value of 4×10^{-5} is typical of 3*d* elements, such as Mn^{3+} ions, and 4*f* elements, such as Ho^{3+} ions. It is worth noting that the nonmonotonic behavior of magnetostriction is only observed at temperatures below $T = 30$ K, i.e., below the temperature of spin reorientation of manganese [6, 7]. We conclude that, in the first approximation, Mn^{3+} ions are responsible for the observed effects. Although, as was mentioned above, the rare-earth metal ions are usually responsible for the behavior of magnetostriction, which is different from the quadratic type. Therefore, we may also assume that the holmium ion determines the shape of striction curves, but, since the effect is observed at temperatures below the spin-reorientation transition of manganese, we may also assume that there is the correlation between manganese and holmium ions. The character of interaction between 3*d* and 4*f* elements remains understudied, although it is of great importance for physics of magnetic phenomena.

To check this conclusion, we performed the measurements on the hexagonal $YMnO_3$ single crystal, the structure of which is the most similar to the investigated $HoMnO_3$ single crystals (Fig. 5) among the compounds without the magnetic 4*f* ion. All the $\Delta L/L(H, T)$ dependences are monotonic in all the experimental configurations. This allows us to conclude that the Ho^{3+} ions determine the behavior of magnetostriction, but only when the magnetic moment of Mn^{3+} ions is parallel to the hexagonal crystal axis ($P\underline{6}3c\underline{m}$ configuration).

Comparison of the magnetostriction plots for the $HoMnO_3$ and $YMnO_3$ single crystals showed that the main source of the investigated effect is the Ho^{3+} subsystem. The magnetostriction in the crystals with 4*f* ions is governed by two different mechanisms: the single-ion magnetostriction caused by the crystal field and the two-ion exchange magnetostriction [30].

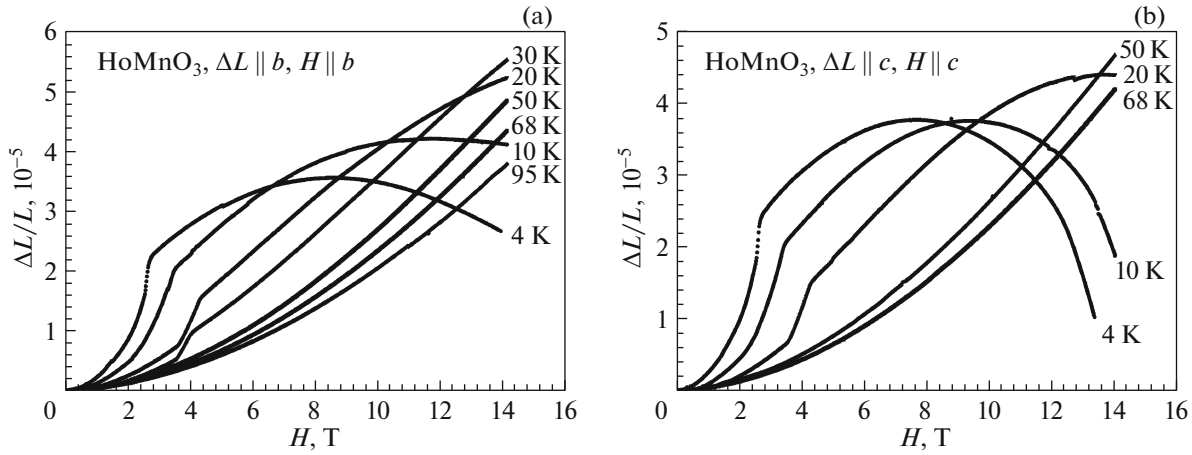

Fig. 4. Longitudinal magnetostriction of $HoMnO_3$ at different temperatures in different configurations.

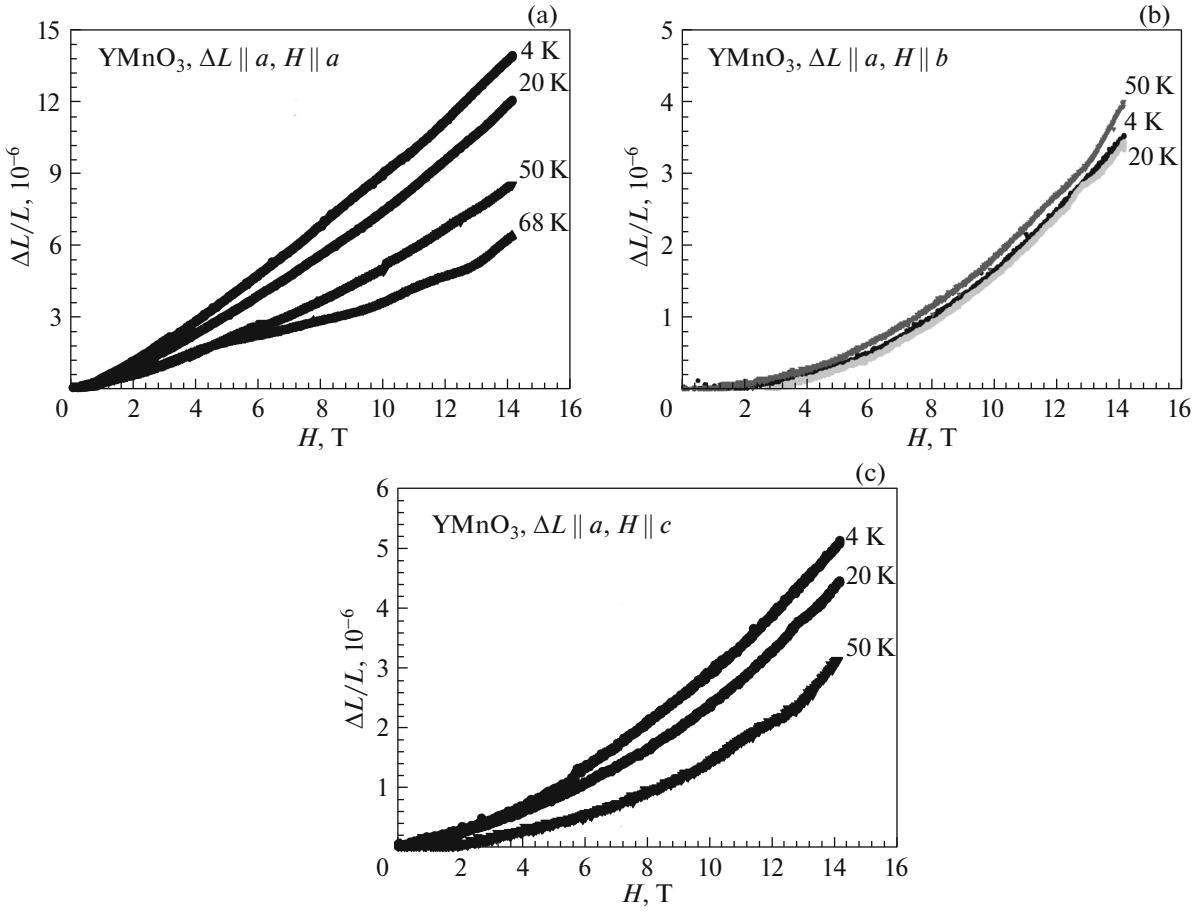

Fig. 5. Transverse and longitudinal magnetostriction of $YMnO_3$ at different temperatures in different configurations.

The R^{3+} ions in hexagonal $RMnO_3$ can occupy two nonequivalent positions. The crystal electric field (CEF) parameters B_l^m for these positions were calculated for $YbMnO_3$ by Diviš et al. [31]. We recalculated the B_l^m parameters of Yb^{3+} to the parameters of Ho^{3+} and obtained a set of CEF parameters for two nonequivalent Ho^{3+} positions.

Fabreges et al. [32] showed that in $YbMnO_3$ the interaction between the Mn^{3+} and Yb^{3+} subsystems can be described by the molecular field of Mn^{3+} ions

affecting the Yb^{3+} subsystem. This molecular field tends to align the Yb^{3+} magnetic moments perpendicular to the Mn^{3+} magnetic moment. We applied this approach to our system and obtained the model Hamiltonian for the Ho subsystem

$$H = \sum B_T^m O_l^m - \sum g_J \mu_B J_i H_{\text{mol}} - \sum g_J \mu_B J_l H_{\text{external}}, \quad (1)$$

where the first term is the contribution of the crystal electric field, the second term describes the interaction between Mn and Ho magnetic subsystems, and the third term is the energy of the external magnetic field.

Using Hamiltonian (1) and McPhase program [http://www.mcphase.de], we calculated the stress tensor components. These components make it possible to qualitatively describe our results on the measured magnetostriction. The results of the calculation are shown in the inset in Fig. 3. Obviously, the calculations for the $L \parallel c$ and $H \parallel b$ at $T = 4$ K configurations agree well with the experimental data. Therefore, we can state that the anomalies in the magnetostriction data are caused by the crystal electric field in the presence of the molecular field of the Mn^{3+} subsystem.

To more deeply understand the magnetostriction behavior, it is necessary to analyze the Ho–Mn interaction in more detail. Our simple model has only a narrow range of applicability, especially considering that we ignored the exchange magnetostriction. Moreover, the crystal-electric-field parameters calculated by us for $HoMnO_3$ from the parameters of $YbMnO_3$ [31] cannot be considered strictly determined; therefore, additional optical or neutron spectroscopy experiments are needed to establish the B_l^m parameters.

4. CONCLUSIONS

We can state that Ho^{3+} ions strongly affect the magnetostriction effects in $HoMnO_3$: these ions affect the coupling mechanism in the hexagonal $HoMnO_3$ single crystal. It is worth noting that the effects were observed in the phase diagram region where Mn^{3+} ions are antiferromagnetically ordered. Further investigations are needed to develop a microscopic model for describing the coupling in the investigated compounds. The interaction between 3*d* and 4*f* ions remains understudied and is of great importance for physics of magnetic phenomena. The $RMnO_3$ hexagonal manganites can be suitable objects for solving this problem.

ACKNOWLEDGMENTS

We thank A.A. Podlesnyak (Oak Bridge National Laboratory) for discussions.

This study was supported by the Russian Foundation for Basic Research, project no. 16-32-00163.

REFERENCES

1. T. Kimura, T. Goto, H. Shintani, and K. Ishizaka, Nature (London, U.K.) **426**, 55 (2003).
2. T. Lottermoser, T. Lonkai, U. Amann, and D. Hohlwein, Nature (London, U.K.) **430**, 541 (2004).
3. M. Fiebig, J. Phys. D **38** (8), R123 (2005).
4. W. Eerenstein, N. D. Mathur, and J. F. Scott, Nature (London, U.K.) **442**, 759 (2006).
5. S. W. Cheong and M. Mostovoy, Nat. Mater. **6**, 13 (2007).
6. F. Yen, C. D. Cruz, B. Lorenz, E. Galstyan, and Y. Y. Sun, J. Mater. Res. **22**, 2163 (2007).
7. B. Lorenz, ISRN Condens. Matter Phys. **2013**, 43 (2013).
8. J. S. Zhou, J. B. Goodenough, J. M. Gallardo-Amores, E. Morán, M. A. Alario-Franco, and R. Caudillo, Phys. Rev. B **74**, 014422 (2006).
9. M. Mostovoy, Nat. Mater. **9**, 188 (2010).
10. O. P. Vajk, M. Kenzelmann, J. W. Lynn, S. B. Kim, and S.-W. Cheong, Phys. Rev. Lett. **94**, 087601 (2005).
11. O. P. Vajk, M. Kenzelmann, J. W. Lynn, S. B. Kim, and S.-W. Cheong, Appl. Phys. **99**, 08E301 (2006).
12. Sh.-Z. Lin, X. Wang, Y. Kamiya, G.-W. Chern, F. Fan, D. Fan, B. Casas, Y. Liu, V. Kiryukhin, W. H. Zurek, C. D. Batista, and S.-W. Cheong, Nat. Phys. **10**, 970 (2014).
13. H. Das, A. L. Wysocki, Y. Geng, W. Wu, and C. J. Fennie, Nat. Commun. **5**, 2998 (2014).
14. M. Fiebig, Th. Lottermoser, and R. V. Pisarev, J. Appl. Phys. **93**, 8194 (2003).
15. N. Lee, Y. J. Choi, M. Ramazanoglu, W. Ratcliff, V. Kiryukhin, and S.-W. Cheong, Phys. Rev. B **84**, 020101(R) (2011).
16. G. Ping, W. WeiTian, Z. Wei, and S. Yu Ming, Sci. China-Phys. Mech. Astron. **57**, 1875 (2014).
17. W. Wang, B. Xu, P. Gao, W. Zhang, and Y. Sun, Solid State Commun. **177**, 7 (2014).
18. B. Khana, H. A. R. Aliabad, N. Razghandi, M. Maqbool, S. J. Asadabadi, and I. Ahmad, Comp. Phys. Commun. **187**, 1 (2015).
19. J. Vermette, S. Jandl, M. Orlita, and M. M. Gospodinov, Phys. Rev. B **85**, 134445 (2012).
20. M. Fiebig, C. Degenhardt, and R. V. Pisarev, J. Appl. Phys. **91**, 8867 (2002).
21. B. Lorenz, A. P. Litvinchuk, M. M. Gospodinov, and C. W. Chu, Phys. Rev. Lett. **92**, 087204 (2004).
22. H. Sugie, N. Iwata, and K. Kohn, J. Phys. Soc. Jpn. **71**, 1558 (2002).
23. S. Nandi, A. Kreyssig, L. Tan, J. W. Kim, J. Q. Yan, J. C. Lang, D. Haskel, R. J. McQueeney, and A. I. Goldman, Phys. Rev. Lett. **100**, 217201 (2008).

24. A. Muñoz, J. A. Alonso, M. J. Martínez-Lope, M. T. Casáis, J. L. Martínez, and M. T. Fernández-Díaz, Chem. Mater. **13**, 1497 (2001).

25. S. Lee, A. Pirogov, M. Kang, K.-H. Jang, M. Yonemura, T. Kamiyama, S.-W. Cheong, F. Gozzo, N. Shin, H. Kimura, Y. Noda, and J.-G. Park, Nature (London, U.K.) **451**, 805 (2008).

26. N. V. Mushnikov and T. Goto, Phys. Rev. B **70**, 054411 (2004).

27. C. Fan, Z. Y. Zhao, J. D. Song, J. C. Wu, F. B. Zhang, and X. F. Sun, J. Cryst. Growth **388**, 54 (2014).

28. A. D. Balaev, Yu. V. Boyarshinov, M. M. Karpenko, and B. P. Khrustalev, Prib. Tekh. Eksp., No. 3, 167 (1985).

29. V. I. Nizhankovskii, Eur. Phys. J. B **71**, 55 (2009).

30. M. Doerr, M. Rotter, and A. Lindbaum, Adv. Phys. **54** (1), 1 (2005).

31. M. Diviš, J. Hölsä, M. Lastusaari, A. P. Litvinchuk, and V. Nekvasil, J. Alloys Compd. **451**, 662 (2008).

32. X. Fabrèges, I. Mirebeau, P. Bonville, S. Petit, G. Lebras-Jasmin, A. Forget, G. André, and S. Pailhès, Phys. Rev. B **78**, 214422 (2008).

Translated by E. Bondareva